Journal of Biological Physics **30:** 239–259, 2004.

Theoretical and Computational Multiple Regression Study of Gastric Electrical Activity Using Dipole Tracing from Magnetic Field Measurements

ANDREI IRIMIA[1], JOHN J. BEAUCHAMP[2] and L. ALAN BRADSHAW[1,*]
[1]*Living State Physics Laboratories, Department of Physics and Astronomy Vanderbilt University, Station B, Box 1807, Nashville, TN, 37235, USA;* [2]*Department of Mathematics, Lipscomb University, 3901 Granny White Pike, Nashville, TN, 37204, USA*
*(*Author for correspondence, e-mail: alan.bradshaw@vanderbilt.edu)*

Abstract. The biomagnetic inverse problem has captured the interest of both mathematicians and physicists due to its important applications in the medical field. As a result of our experience in analyzing the electrical activity of the gastric smooth muscle, we present here a theoretical model of the magnetic field in the stomach and a computational implementation whereby we demonstrate its realism and usefulness. The computational algorithm developed for this purpose consists of dividing the magnetic field signal input surface into centroid-based grids that allow recursive least-squares approximations to be applied, followed by comparison tests in which the locations of the best-fitting current dipoles are determined. In the second part of the article, we develop a multiple-regression analysis of experimental gastric magnetic data collected using Superconducting QUantum Interference Device (SQUID) magnetometers and successfully processed using our algorithm. As a result of our analysis, we conclude on statistical grounds that it is sufficient to model the electrical activity of the GI tract using only two electric current dipoles in order to account for the magnetic data recorded non-invasively with SQUID magnetometers above the human abdomen.

Key words: gastrointestinal electrical activity, biomagnetic inverse problem, current dipole

1. Introduction

Bioelectric currents in the gastrointestinal (GI) tract have been the focus of active research in recent years due to the demonstrated possibility [3–4, 19] to detect a number of pathological conditions of the stomach and intestine by performing experimental studies of abnormal bioelectric current propagation, particularly using Superconducting QUantum Interference Device magnetometers (SQUIDs). In the stomach and small bowel, electric currents due to the presence of transmembrane potentials exhibit propagation patterns, which are also present throughout the rest of the GI tract. This phenomenon consists of depolarization and repolarization waves

that advance along the corpus of the stomach as a result of the presence of coupled cells in the smooth muscle of the tract. In the case of stomach, this property of gastric tissues allows the organ to behave like an electric syncytium and also gives rise to electric current propagation. The frequency of the gastric electrical activity (GEA) varies greatly depending upon the portion of the tract analyzed, the health state of the organ, and upon other tissue characteristics.

Experimentally, bioelectric currents are ordinarily detected using methods such as the electrogastrogram (EGG). In recent years, however, a number of inherent difficulties of the method—such as the dependence of electric recordings on tissue conductivity—have suggested the use of the magnetogastrogram (MGG) instead, since magnetic fields are dependent on tissue permeability, which is nearly the same as that of free space. Due to the fact that gastric biomagnetic fields are relatively weak—with strengths of the order of 10^{-12} T—a highly sensitive measurement apparatus is required for experimental data collection, such as the SQUID biomagnetometer. In order to determine the electric current distribution in the stomach using magnetic field recordings, one must solve the biomagnetic inverse problem, which consists of obtaining either analytical or numerical solutions for the electric potential V and current density $\mathbf{J}$ based on measurements of the magnetic field $\mathbf{B}$. Great difficulties can be associated with this because solutions to the inverse problem are not unique; moreover, from a biophysical perspective, only those solutions that have the property of being anatomically relevant are of interest. As we shall explain later, the GEA can be modeled using one or more current dipoles that are assumed to produce the magnetic field recorded by the magnetometer. We believe that this article is the first one to present investigative results concerning the GEA obtained using an inverse biomagnetic method that involves current dipole tracing.

Numerous methods have been designed for solving the inverse problem based on various *a priori* information concerning the current distribution. Typically, modeling the phenomenon of bioelectric current propagation can be done using the mathematical tools of the quasistatic approximation. In particular, the concept of the electric current dipole has proven to be very effective in describing the physiology of electrically active biological tissues [5, 14, 15, 25]. Very often, one such single dipole is sufficient for capturing the essential characteristics of the current source. For example, this is feasible for the brain [2], where a single dipole is usually appropriate in many investigations. In the case of GI current propagation, a large number of dipoles are present in the abdomen, and including *a priori* information can be very difficult. Moreover, because of the size and anatomic configuration of the GI tract, formulating theoretical models involving the propagation of multiple dipoles and predicting relevant information concerning abnormal electrical activity using these models are two goals whose achievement is both necessary and difficult. In the pages that follow, we present a mathematical method for overcoming some of these obstacles, particularly with respect to the issue of modeling GI electrical activity both qualitatively and quantitatively. We then present a numerical algorithm that implements this model using an inverse procedure. Finally, by performing a

statistical multiple-regression analysis of GI magnetic field data collected using SQUID magnetometers, the validity of the theoretical assumptions in our model will be considered and directions for further investigation will be discussed.

2. Theoretical Model

The electric fields of the human GI tract are produced due to the presence of propagating waves that oscillate in a cyclic pattern. Depending on the region of their location along the tract, these waves exhibit various frequencies, i.e. $\sim$3 cycles min^{-1} in the stomach and $\sim$12 cycles min^{-1} in the proximal duodenum [1], for example. Due to the anatomical structure of these two organs, the propagation of electric currents can be modeled as a circular isopotential loop of current dipoles. By taking advantage of the nature of the GI tract, one can express this potential in two dimensions as a function of position $\mathbf{r}$ and time t in the form

$$V(\mathbf{r}, t) = u_s(\lambda)V_\alpha(\rho, \theta, t), \tag{1}$$

where we employ cylindrical coordinates denoted by ρ, θ and multiply the unit step function u_s at the leading edge λ of the ring by the waveform V_α of the membrane potential. Of great importance here is the relationship between the potential inside the muscle cell—V_c ($\mathbf{r}$, t)—and the potential of the (extracellular) membrane V_α defined above, which can be expressed through the formula

$$V_\text{c}(\mathbf{r}, t) = \frac{r_\text{i}}{r_\text{i} + r_\text{o}} V_\alpha, \tag{2}$$

where r_i and r_o are the resistivities of the cell interior and exterior, respectively. Ohm's law can be employed to obtain the intracellular current as

$$\mathbf{J}_\text{c}(\mathbf{r}, t) = \frac{\boldsymbol{\nabla} V_\text{c}(\mathbf{r}, t)}{r_\text{i}}. \tag{3}$$

This expression implies that gastric current propagation can be modeled as a ring of leading edge depolarization dipoles. In addition to presuming that the stomach is essentially a homogeneous organ located inside the abdomen, the assumption of a bounded medium can also be made. To obtain an analytical expression for the magnetic field given these two characteristics, a well-chosen form of the Biot-Savart law can be used. Since the theoretical background concerning this aspect of the problem has already been extensively discussed elsewhere [9–11, 23], we briefly summarize here the mathematical model and physical assumptions behind our inverse method for describing GI $\mathbf{B}$ fields. Letting γ represent the domain of integration over a region of the body, a current dipole defined as

$$\mathbf{Q} \equiv \iiint_\gamma \mathbf{J}(\mathbf{r}')\text{d}^3\text{r}' \tag{4}$$

allows the law of Biot and Savart to be written in the computationally advantageous form

$$\mathbf{B}(\mathbf{r}) \cong \frac{\mu}{4\pi}\mathbf{Q} \times \frac{(\mathbf{r}-\mathbf{r}')}{|\mathbf{r}-\mathbf{r}'|^3}, \tag{5}$$

where the current dipole is a good approximation of the magnetic field source. This formula is beneficial both analytically and computationally, because it allows us to redefine the inverse biomagnetic problem in terms of identifying the location and orientation of the current dipole $\mathbf{Q}$ given by the so-called elemental dipoles Q_x, Q_y, and Q_z:

$$\mathbf{Q} = Q_x + Q_y + Q_z \tag{6}$$

$$= \begin{pmatrix} Q_x \\ 0 \\ 0 \end{pmatrix} + \begin{pmatrix} 0 \\ Q_y \\ 0 \end{pmatrix} + \begin{pmatrix} 0 \\ 0 \\ Q_z \end{pmatrix} \tag{7}$$

This linear model can be useful especially from a computational perspective. Returning to the task of solving the biomagnetic inverse problem using the formalism developed thus far, it can be shown that the gastrointestinal isopotential ring of depolarization/repolarization dipoles can be well approximated by a single dipole located in the plane of the ring within the cylinder, conoid or ellipsoid used to model the GI tract. By making use of the Biot-Savart law, the vector components of the magnetic field outside the body can be evaluated using the current dipole expression

$$\mathbf{B}(\mathbf{r}) \cong \frac{\mu_0}{4\pi}\mathbf{Q} \times \frac{(\mathbf{r}-\mathbf{r}')}{|\mathbf{r}-\mathbf{r}'|^3} \tag{8}$$

$$= \frac{\mu_0}{4\pi}\frac{1}{|r-r'|^3}\begin{vmatrix} \mathbf{i} & \mathbf{j} & \mathbf{k} \\ Q_x & Q_y & Q_z \\ x-x_0 & y-y_0 & z-z_0 \end{vmatrix} \tag{9}$$

$$= \frac{\mu_0}{4\pi}\frac{1}{|\mathbf{r}-\mathbf{r}'|^3}\{[Q_y(z-z_0) - Q_z(y-y_0)]\mathbf{i} + [Q_z(x-x_0) - Q_x(z-z_0)]\mathbf{j} + [Q_x(y-y_0) - Q_y(x-x_0)]\mathbf{k}\} \tag{10}$$

As it has already been stated, one important difficulty related to the biomagnetic inverse problem is that its solutions are not unique. For example, if we wished to use the expressions above to form a system of simultaneous linear equations

$$\frac{\mu_0}{4\pi}\frac{1}{|\mathbf{r}-\mathbf{r}'|^3}\begin{pmatrix} 0 & z-z_0 & -(y-y_0) \\ -(z-z_0) & 0 & (x-x_0) \\ y-y_0 & -(x-x_0) & 0 \end{pmatrix}\begin{pmatrix} Q_x \\ Q_y \\ Q_z \end{pmatrix} = \begin{pmatrix} B_x \\ B_y \\ B_z \end{pmatrix}, \tag{11}$$

we would immediately notice that there are an infinite number of solutions due to the fact that a parameter must be specified in order to solve it. We must therefore find another way to determine the orientation of the current dipole based on the information specified by the magnetic field recordings. The technique employed here is to perform a least-squares approximation of the vector components of $\mathbf{Q}$ so that the squared differences between the recorded and computed values of the magnetic field are minimized. Before this is done, we shall assume that the magnetic field recorded experimentally is due to two dipoles, one located in the stomach ($\widehat{\mathbf{Q}}$) and another one in the intestine ($\breve{\mathbf{Q}}$). This two-dipole model is obviously better than a single-dipole model both anatomically and statistically because more sources of current are accounted for in the simulation. However, for the purpose of demonstrating the necessity of using two dipoles instead of one for modeling GI electrical activity, we will also present the results of our regression analysis for a single dipole model. As it will be shown in the second part of this article using a statistical analysis of experimental data, a model involving two dipoles is indeed necessary. Explaining abdominal magnetic field recordings using one dipole for the stomach and another for the intestine is the simplest way to account for the recorded magnetic fields and also offers an excellent motivation to continue our study of GI biomagnetism based on this model. In the pages that follow, the mathematical formalism that is developed refers to the two-dipole model only, as the latter is a natural extension of the simpler regression model involving a single dipole. Although a two-dipole model cannot be justified physiologically due to the very large number of current sources present in the human abdomen, our present article constitutes the first attempt to study the GEA from inverse solutions of the magnetic field using more than one dipole.

3. Computational Procedure

To obtain solutions to the inverse problem of biomagnetism using experimentally measured $\mathbf{B}$ fields, we have developed a computational procedure particularly suitable to the anatomy of the stomach as well as to our data acquisition methods. The area corresponding to the co-planar input channels of the magnetometer can be divided into an $\alpha \times \beta$ grid, where α and β should be chosen according to the spatial

resolution desired. In accordance with vector addition rules, the total magnetic field recorded is the sum of the magnetic fields due to the individual n dipoles assumed in the model (two in our simplified case):

$$\mathbf{B} \cong \frac{\mu_0}{4\pi} \sum_{i=1}^{n} \frac{1}{\|\mathbf{r} - \mathbf{r}_i'\|^3} \mathbf{Q}_i \times (\mathbf{r} - \mathbf{r}_i') = \widehat{\mathbf{B}} + \breve{\mathbf{B}}, \tag{12}$$

where $\widehat{\mathbf{B}}$ is the magnetic field due to the gastric dipole and $\breve{\mathbf{B}}$ is due to the intestinal dipole. From this point forward, it shall be assumed that $\tilde{\mathbf{B}}$ refers to the magnetic field value measured experimentally. For the two-dipole model, the sum of values to be minimized over the entire input grid thus becomes

$$\sum_{i=1}^{\alpha} \sum_{j=1}^{\beta} [\tilde{\mathbf{B}}_{ij}(\mathbf{r}) - \mathbf{B}_{ij}(\mathbf{r})]^2 = \sum_{i=1}^{\alpha} \sum_{j=1}^{\beta} [\tilde{\mathbf{B}}_{ij}(\mathbf{r}) - \widehat{\mathbf{B}}_{ij}(\mathbf{r}) - \breve{\mathbf{B}}_{ij}(\mathbf{r})]^2, \tag{13}$$

where double summation is performed over the entire set of grid nodes. To identify the best-fitting orientation of each current dipole, partial differentiation of the magnetic field expression must be performed with respect to each of the dipole vector components. Minimization of the vector component of $\mathbf{B}$ in the $\hat{\mathbf{i}}$ direction thus yields

$$\begin{aligned} 0 &= \frac{\partial}{\partial \widehat{Q}_y} \sum_{i=1}^{\alpha} \sum_{j=1}^{\beta} [\tilde{B}_x(y,z)|_{ij} - \widehat{B}_x(y,z)|_{ij} - \breve{B}_x(y,z)|_{ij}]^2 \\ &= \sum_{i=1}^{\alpha} \sum_{j=1}^{\beta} 2[\tilde{B}_x(y,z)|_{ij} - \widehat{B}_x(y,z)|_{ij} - \breve{B}_x(y,z)|_{ij}] \frac{\mu_0}{4\pi} \frac{1}{|\tilde{\mathbf{r}}_{ij} - \widehat{\mathbf{r}}'|^3} (z_{ij} - \widehat{z}_0) \end{aligned} \tag{14}$$

$$\begin{aligned} 0 &= \frac{\partial}{\partial \widehat{Q}_z} \sum_{i=1}^{\alpha} \sum_{j=1}^{\beta} [\tilde{B}_x(y,z)|_{ij} - \widehat{B}_x(y,z)|_{ij} - \breve{B}_x(y,z)|_{ij}]^2 \\ &= \sum_{i=1}^{\alpha} \sum_{j=1}^{\beta} 2[\tilde{B}_x(y,z)|_{ij} - \widehat{B}_x(y,z)|_{ij} - \breve{B}_x(y,z)|_{ij}] \frac{\mu_0}{4\pi} \frac{-1}{|\mathbf{r}_{ij} - \widehat{\mathbf{r}}'|^3} (y_{ij} - \widehat{y}_0) \end{aligned} \tag{15}$$

$$\begin{aligned} 0 &= \frac{\partial}{\partial \widehat{Q}_y} \sum_{i=1}^{\alpha} \sum_{j=1}^{\beta} [\tilde{B}_x(y,z)|_{ij} - \widehat{B}_x(y,z)|_{ij} - \breve{B}_x(y,z)|_{ij}]^2 \\ &= \sum_{i=1}^{\alpha} \sum_{j=1}^{\beta} 2[\tilde{B}_x(y,z)|_{ij} - \widehat{B}_x(y,z)|_{ij} - \breve{B}_x(y,z)|_{ij}] \frac{\mu_0}{4\pi} \frac{1}{|\mathbf{r}_{ij} - \widehat{\mathbf{r}}'|^3} (z_{ij} - \breve{z}_0) \end{aligned} \tag{16}$$

$$0 = \frac{\partial}{\partial \breve{Q}_z} \sum_{i=1}^{\alpha} \sum_{j=1}^{\beta} [\tilde{B}_x(y,z)|_{ij} - \hat{B}_x(y,z)|_{ij} - \breve{B}_x(y,z)|_{ij}]^2$$

$$= \sum_{i=1}^{\alpha} \sum_{j=1}^{\beta} 2[\tilde{B}_x(y,z)|_{ij} - \hat{B}_x(y,z)|_{ij} - \breve{B}_x(y,z)|_{ij}] \frac{\mu_0}{4\pi} \frac{-1}{|\mathbf{r}_{ij} - \breve{\mathbf{r}}'|^3} (y_{ij} - \breve{y}_0) \tag{17}$$

After inserting the expressions for B_x into the equalities above and multiplying out the terms, the set of simultaneous linear equations to be solved is obtained:

$$\sum_{i=1}^{m} \sum_{j=1}^{n} \frac{(\hat{y}_{ij} - \hat{y}_0)(\hat{x}_{ij} - \hat{x}_0)}{\|\hat{\mathbf{r}}_{ij} - \hat{\mathbf{r}}_0\|^6} \hat{Q}_x - \sum_{i=1}^{m} \sum_{j=1}^{n} \frac{(\hat{x}_{ij} - \hat{x}_0)^2}{\|\hat{\mathbf{r}}_{ij} - \hat{\mathbf{r}}_0\|^6} \hat{Q}_y$$

$$+ \sum_{i=1}^{m} \sum_{j=1}^{n} \frac{(\hat{x}_{ij} - \hat{x}_0)(\breve{y}_{ij} - \breve{y}_0)}{\|\hat{\mathbf{r}}_{ij} - \hat{\mathbf{r}}_0\|^3 \|\breve{\mathbf{r}}_{ij} - \breve{\mathbf{r}}_0\|^3} \breve{Q}_x - \sum_{i=1}^{m} \sum_{j=1}^{n} \frac{(\hat{x}_{ij} - \hat{x}_0)(\breve{x}_{ij} - \breve{x}_0)}{\|\hat{\mathbf{r}}_{ij} - \hat{\mathbf{r}}_0\|^3 \|\breve{\mathbf{r}}_{ij} - \hat{\mathbf{r}}_0\|^3} \breve{Q}_y$$

$$= \frac{1}{\eta} \sum_{i=1}^{m} \sum_{j=1}^{n} \frac{(\hat{x}_{ij} - \hat{x}_0)}{\|\hat{\mathbf{r}}_{ij} - \hat{\mathbf{r}}_0\|^3} \tilde{B}_{zij} \tag{18}$$

$$\sum_{i=1}^{m} \sum_{j=1}^{n} \frac{(\hat{y}_{ij} - \hat{y}_0)^2}{\|\hat{\mathbf{r}}_{ij} - \hat{\mathbf{r}}_0\|^6} \hat{Q}_x - \sum_{i=1}^{m} \sum_{j=1}^{n} \frac{(\hat{x}_{ij} - \hat{x}_0)(\breve{y}_{ij} - \breve{y}_0)}{\|\hat{\mathbf{r}}_{ij} - \hat{\mathbf{r}}_0\|^6} \hat{Q}_y$$

$$+ \sum_{i=1}^{m} \sum_{j=1}^{n} \frac{(\hat{y}_{ij} - \hat{y}_0)(\breve{y}_{ij} - \breve{y}_0)}{\|\hat{\mathbf{r}}_{ij} - \hat{\mathbf{r}}_0\|^3 \|\breve{\mathbf{r}}_{ij} - \breve{\mathbf{r}}_0\|^3} \breve{Q}_x - \sum_{i=1}^{m} \sum_{j=1}^{n} \frac{(\hat{y}_{ij} - \hat{y}_0)(\breve{x}_{ij} - \breve{x}_0)}{\|\hat{\mathbf{r}}_{ij} - \hat{\mathbf{r}}_0\|^3 \|\breve{\mathbf{r}}_{ij} - \breve{\mathbf{r}}_0\|^3} \breve{Q}_y$$

$$= \frac{1}{\eta} \sum_{i=1}^{m} \sum_{j=1}^{n} \frac{(\hat{y}_{ij} - \hat{y}_0)}{\|\hat{\mathbf{r}}_{ij} - \hat{\mathbf{r}}_0\|^3} \tilde{B}_{zij} \tag{19}$$

$$\sum_{i=1}^{m} \sum_{j=1}^{n} \frac{(\hat{y}_{ij} - \hat{y}_0)(\breve{x}_{ij} - \breve{x}_0)}{\|\hat{\mathbf{r}}_{ij} - \hat{\mathbf{r}}_0\|^3 \|\breve{\mathbf{r}}_{ij} - \breve{\mathbf{r}}_0\|^3} \hat{Q}_x - \sum_{i=1}^{m} \sum_{j=1}^{n} \frac{(\hat{x}_{ij} - \hat{x}_0)(\breve{x}_{ij} - \breve{x}_0)}{\|\hat{\mathbf{r}}_{ij} - \hat{\mathbf{r}}_0\|^3 \|\breve{\mathbf{r}}_{ij} - \breve{\mathbf{r}}_0\|^3} \hat{Q}_y$$

$$+ \sum_{i=1}^{m} \sum_{j=1}^{n} \frac{(\breve{x}_{ij} - \breve{x}_0)(\breve{y}_{ij} - \breve{y}_0)}{\|\breve{\mathbf{r}}_{ij} - \breve{\mathbf{r}}_0\|^6} \breve{Q}_x - \sum_{i=1}^{m} \sum_{j=1}^{n} \frac{(\breve{x}_{ij} - \breve{x}_0)^2}{\|\breve{\mathbf{r}}_{ij} - \breve{\mathbf{r}}_0\|^6} \breve{Q}_y$$

$$= \frac{1}{\eta} \sum_{i=1}^{m} \sum_{j=1}^{n} \frac{(\breve{x}_{ij} - \breve{x}_0)}{\|\breve{\mathbf{r}}_{ij} - \breve{\mathbf{r}}_0\|^3} \tilde{B}_{zij} \tag{20}$$

$$\sum_{i=1}^{m}\sum_{j=1}^{n}\frac{(\widehat{y}_{ij}-\widehat{y}_0)(\breve{y}_{ij}-\breve{y}_0)}{\|\widehat{\mathbf{r}}_{ij}-\widehat{\mathbf{r}}_0\|^3\|\breve{\mathbf{r}}_{ij}-\breve{\mathbf{r}}_0\|^3}\widehat{Q}_x-\sum_{i=1}^{m}\sum_{j=1}^{n}\frac{(\widehat{x}_{ij}-\widehat{x}_0)(\breve{y}_{ij}-\breve{y}_0)}{\|\widehat{\mathbf{r}}_{ij}-\widehat{\mathbf{r}}_0\|^3\|\breve{\mathbf{r}}_{ij}-\breve{\mathbf{r}}_0\|^3}\widehat{Q}_y$$

$$+\sum_{i=1}^{m}\sum_{j=1}^{n}\frac{(\breve{y}_{ij}-\breve{y}_0)^2}{\|\breve{\mathbf{r}}_{ij}-\breve{\mathbf{r}}_0\|^6}\breve{Q}_x-\sum_{i=1}^{m}\sum_{j=1}^{n}\frac{(\breve{x}_{ij}-\breve{x}_0)(\breve{y}_{ij}-\breve{y}_0)}{\|\breve{\mathbf{r}}_{ij}-\breve{\mathbf{r}}_0\|^6}\breve{Q}_y$$

$$=\frac{1}{\eta}\sum_{i=1}^{m}\sum_{j=1}^{n}\frac{(\breve{y}_{ij}-\breve{y}_0)}{\|\breve{\mathbf{r}}_{ij}-\breve{\mathbf{r}}_0\|^3}\tilde{B}_{zij} \tag{21}$$

where $\eta \equiv \mu_0(4\pi)^{-1}$. Equations (18)–(21) form what is typically called the normal set of equations for the regression model. If the expressions above are carefully ordered, it becomes evident that the system can be expressed as the product of several matrices. For convenience of notation, let us define the double summation symbol $\xi_{\alpha\beta}$ over a two-dimensional grid such that

$$\xi_{\alpha\beta}\phi_{ij}=\sum_{i=1}^{\alpha}\sum_{i=1}^{\beta}\phi_{ij}, \tag{22}$$

where we assume that α and β have the same meaning as explained above. Solving the system of equations then becomes equivalent to the process of finding solutions to the matrix equation

$$\mathbf{TAWQ}=\frac{1}{\eta}\mathbf{UB} \tag{23}$$

in which

$$\mathbf{T}=\begin{pmatrix}1 & & & \\ & -1 & & \\ & & 1 & \\ & & & -1\end{pmatrix} \tag{24}$$

$$\mathbf{A}=\begin{pmatrix}\xi_{\alpha\beta}(\widehat{y}_{ij}-\widehat{y}_0)\ \|\widehat{\mathbf{r}}_{ij}-\widehat{\mathbf{r}}_0\|^{-3}\\ \xi_{\alpha\beta}(\widehat{x}_{ij}-\widehat{x}_0)\ \|\widehat{\mathbf{r}}_{ij}-\widehat{\mathbf{r}}_0\|^{-3}\\ \xi_{\alpha\beta}(\breve{y}_{ij}-\breve{y}_0)\ \|\breve{\mathbf{r}}_{ij}-\breve{\mathbf{r}}_0\|^{-3}\\ \xi_{\alpha\beta}(\widehat{x}_{ij}-\widehat{x}_0)\ \|\breve{\mathbf{r}}_{ij}-\breve{\mathbf{r}}_0\|^{-3}\end{pmatrix} \tag{25}$$

$$\mathbf{W}=\begin{pmatrix}\xi_{\alpha\beta}\dfrac{(\widehat{x}_{ij}-\widehat{x}_0)}{\|\widehat{\mathbf{r}}_{ij}-\widehat{\mathbf{r}}_0\|^3} & \xi_{\alpha\beta}\dfrac{(\widehat{y}_{ij}-\widehat{y}_0)}{\|\widehat{\mathbf{r}}_{ij}-\widehat{\mathbf{r}}_0\|^3} & \xi_{\alpha\beta}\dfrac{(\breve{x}_{ij}-\breve{x}_0)}{\|\breve{\mathbf{r}}_{ij}-\breve{\mathbf{r}}_0\|^3} & \xi_{\alpha\beta}\dfrac{(\breve{y}_{ij}-\breve{y}_0)}{\|\breve{\mathbf{r}}_{ij}-\breve{\mathbf{r}}_0\|^3}\end{pmatrix} \tag{26}$$

$$\mathbf{Q} = \begin{pmatrix} \widehat{Q}_x \\ \widehat{Q}_y \\ \breve{Q}_x \\ \breve{Q}_y \end{pmatrix} \tag{27}$$

$$\mathbf{B} = \begin{pmatrix} \xi_{\alpha\beta}\tilde{\mathrm{B}}_{zij} \\ \xi_{\alpha\beta}\tilde{\mathrm{B}}_{zij} \\ \xi_{\alpha\beta}\tilde{\mathrm{B}}_{zij} \\ \xi_{\alpha\beta}\tilde{\mathrm{B}}_{zij} \end{pmatrix} \tag{28}$$

where $B_{zij} \equiv B_z(x, y)|_{ij}$, i.e. the value of B_z evaluated at the grid node denoted by subscripts i and j. Notice that all entries in the matrices (25), (26) and (28) are summations of the respective terms over the entire grid that extends from 1 to α and from 1 to β in two-dimensional space. The column vector **B** corresponds to the observations and **Q** to the parameters to be estimated. By reducing this matrix that defines the system of equations to row echelon form, the best fitting orientation of the current dipole is identified. Due to the presence of $\|\widehat{\mathbf{r}}_{ij} - \widehat{\mathbf{r}}'\|^{-3}$ and $\|\breve{\mathbf{r}}_{ij} - \breve{\mathbf{r}}'\|^{-3}$ in the systems of equations above in **A** and **W**, this can be considered to be a third-order linear model involving a reciprocal and square-root transformation of the independent variables [6, 24] due to the fact that, in Cartesian coordinates,

$$\|\mathbf{r}_{ij} - \mathbf{r}'\|^{-3} = \frac{1}{[\sqrt{(x_{ij} - x_0)^2 + (y_{ij} - y_0)^2 + (z_{ij} - z_0)^2}]^3}. \tag{29}$$

The mathematical formalism developed thus far will now be used to construct a method that identifies the location of the current dipole with sufficient spatial resolution. Before this is done let us define the co-planar nodes of the input grid matrices $\mathbf{G}_x$, $\mathbf{G}_y$ and $\mathbf{G}_z$, where magnetic field values are sampled as

$$\mathbf{G}_x = \begin{pmatrix} B_{x11} & \cdots & B_{x1\beta} \\ \vdots & \ddots & \vdots \\ B_{x\alpha 1} & \cdots & B_{x\alpha\beta} \end{pmatrix}, \tag{30}$$

$$\mathbf{G}_y = \begin{pmatrix} B_{y11} & \cdots & B_{y1\beta} \\ \vdots & \ddots & \vdots \\ B_{y\alpha 1} & \cdots & B_{y\alpha\beta} \end{pmatrix}, \tag{31}$$

$$\mathbf{G}_z = \begin{pmatrix} B_{z11} & \cdots & B_{z1\beta} \\ \vdots & \ddots & \vdots \\ B_{z\alpha 1} & \cdots & B_{z\alpha\beta} \end{pmatrix}, \tag{32}$$

If symmetry is assumed with respect to one of the axes—the x_i axis in a generalized notation—then the grid can be conveniently split into two subdivisions of equal area. In the GI biomagnetic model, the upper subdivision can be assumed to represent a region above the stomach while the lower one corresponds to an area above the small intestine. The possible locations of the gastric and intestinal dipoles can therefore be searched within the corresponding subdivision. In the case of a single dipole model, the entire grid is scanned. By dividing each of the gastric and intestinal grids into smaller ones, the location of the two dipoles can be identified by performing the least squares approximation described above in a combinatorial fashion for all possible dipoles, which are assumed to be located at the centroids of these sub-grids. After the best-fitting combination of sub-grids is identified, the process can be continued by dividing the grid until smaller divisions are no longer available, i.e. the best-fitting node has been identified.

In order to construct formalism for identifying the best-fitting current dipole positions among any possible locations on the grid, let the partition mapping function Ψ be defined recursively as

$$\Psi(\Omega) = \varsigma_\Omega \Psi(\Omega - 1) = \prod_{i=1}^{\alpha} \varsigma_i \quad \text{where } \Omega \in [1,\ \lambda] \text{ and } \Omega \in N^* \tag{33}$$

where $\varsigma_1 = 2$ and the values of $\varsigma_2, \varsigma_3, \ldots, \varsigma_\Omega$ are to be chosen depending on the size and configuration of this two-dimensional matrix. In other words, Ψ defines how the two-dimensional matrix is to be partitioned, where the total number of partitions depends on the level of resolution desired in the iterative process. The variable Ω denotes the level of recursive division, i.e. how many times the original grid has been divided, while the coefficients $\varsigma_1, \varsigma_2, \varsigma_3, \ldots, \varsigma_\Omega$ denote the number of subdivisions for each subgrid at that level. The interval in which the values of Ω are defined ranges from 1 (in which case the grid is divided in only two sectors) to an integer λ which is dependent of how $\varsigma_2, \varsigma_3, \ldots, \varsigma_\Omega$ are selected. The total number of subdivisions, however, may not exceed the total number of grid nodes. If one lets p denote the number of nodes in the grid, this implies that the condition

$$\Psi(\lambda) = \prod_{i=1}^{\lambda} \Omega_i \leq p \tag{34}$$

must apply to the partition function. The process of identifying the locations on the grid for the assumed positions of gastric and intestinal dipoles during the least-squares approximation procedure must involve a rigorous analysis because the

spatial resolution of the algorithm is dependent on this aspect of the method. For each of the Ω subgrids, the expected position of the current dipole corresponds to the centroid of that sub-grid, if the assumption is made that the dipole is located in it. Therefore, for each subgrid, the expected position of the dipole must be computed. For example, this is done for a circle by applying standard center-of-mass formulas [13] and performing integration with respect to the two variables x and y for the n-th region bound by subgrid subscripts a_n and b_n in the x-y plane, i.e.

$$\langle x_n \rangle = \frac{\int_{a_n}^{b_n} x\sqrt{1-x^2}\mathrm{d}x}{\int_{a_n}^{b_n} \sqrt{1-x^2}\mathrm{d}x} \tag{35}$$

and

$$\langle y_n \rangle = \frac{\frac{1}{2}\int_{a_n}^{b_n} (1-x^2)\mathrm{d}x}{\int_{a_n}^{b_n} \sqrt{1-x^2}\mathrm{d}x}, \tag{36}$$

where a_n and b_n represent the x-coordinate extremities of the n-th subgrid within the circle. This ensures that the most likely position is assumed for the dipole in the absence of *a priori* information. At the $(\Omega + 1)$-th recursion level, the corresponding centroids of the smaller grid segments must also be computed in a similar fashion. If there is no anatomical information concerning the region of current propagation, the random variable denoting the true position of the dipole can be thought to obey a continuous uniform distribution such that

$$Q\,(x,\,y) \sim U\,(a,b,c,d) \qquad x \in [a,\,b] \quad \text{and} \quad y \in [c,\,d]\,, \tag{37}$$

where a, b, c and d refer to the world-coordinate extremities of the subgrid in the x and y directions, such that the dipole is equally likely to be located anywhere on it. To identify the best-fitting location numerically with an arbitrary degree of precision, the number of grid nodes should be allowed to increase by virtue of the fact that

$$\lim_{\substack{\alpha\to\infty \\ \beta\to\infty}} \sqrt{(x_i - x)^2 + (y_j - y)^2} = 0, \tag{38}$$

where $(x_i,\, y_j)$ denote the coordinates of the grid node closest to the true dipole at $(x,\, y)$.This implies that the distance from the true location $(x,\, y)$ of the dipole to the nearest grid node $(x_i,\, y_j)$ should be equal to or less than a chosen value ε. As the number of nodes increases, the discrete uniform distribution of the possible dipole location can be used more and more successfully to model the continuous uniform distribution of the true position.

The mathematical procedure described above can be used to identify one current dipole in a given axisymmetric grid. In order to extend this method to the case in which one gastric and one intestinal dipole must be identified simultaneously, it suffices to perform a combinatorial scan in which all the possible combinations of sub-grid centroids in the upper and lower portions of the original grid must be examined. The total number of least squares approximations δ that must be performed in this case is equal to the product of the number of locations to be considered in the upper and lower portions of the grid. Since the grid is assumed to be symmetric with respect to one of the axes, this implies that

$$\delta = \sum_{i=1}^{\lambda} \left[\begin{pmatrix} \frac{1}{2}\Psi(\Omega_i) \\ 1 \end{pmatrix} \begin{pmatrix} \frac{1}{2}\Psi(\Omega_i) \\ 1 \end{pmatrix} \right], \tag{39}$$

$$= \sum_{i=1}^{\lambda} \left[\begin{pmatrix} \frac{1}{4}\Psi^2(\Omega_i) \\ 1 \end{pmatrix} \right] \tag{40}$$

$$= \left(\frac{1}{4}\right)^{\lambda} \left[\sum_{i=1}^{\lambda} \Psi^2(\Omega_i) \right] \tag{41}$$

which implies that the manner in which the grid is partitioned has a great influence upon the number of computations to be performed. If division is performed such that

$$\varsigma_1 = \varsigma_2 = \cdots = \varsigma_\Omega = 2, \tag{42}$$

then

$$\Psi(\Omega) = 2^{\Omega}, \tag{43}$$

and the number of least-squares approximations as a function of grid dimensions behaves logarithmically:

$$\delta(\alpha, \beta) = \mathrm{O}[\log_2(\alpha \cdot \beta)], \tag{44}$$

where Big-Oh notation is used to express the rate of growth for δ. This detail is of great importance because it implies that the dipole identification algorithm described above can be efficient even for very dense grids if $\varsigma_1, \varsigma_2, \varsigma_3, \ldots, \varsigma_\Omega$ are well chosen. The main disadvantage of dividing the grid using a logarithmically-increasing algorithm is that spatial resolution may be compromised if this is not done carefully. In a majority of cases related to GI research, the uniform distribution of sources is only a convenient assumption, especially in the case of the gastric dipole. Grid division must therefore be performed so that a sufficiently spread out section of the grid is scanned before identifying the best-fitting dipoles. On the other hand,

scanning the grid at a large number of positions produces a tremendous increase in the time needed by the algorithm to complete its task. The optimization problem that is apparent here should be solved based on case-specific information such as the real-life size of the input grid and possible reasons for omitting certain grid sectors from the scan.

4. Results

In order to determine the proportion of total variation about the mean $\langle \tilde{\mathbf{B}}_z \rangle$ explained by the regression model adopted in light of the known characteristics of the GI electric current propagation mechanism, we performed an analysis based on experimental data consisting of magnetic field values sampled from a healthy human stomach at a frequency of 200 Hz using the SQUID biomagnetometer (Tristan Technologies, Inc., San Diego, CA) in the Biomagnetism Laboratory at Vanderbilt University. In our experiment, the human subject was placed in supine position with the abdomen immediately below the input coils of the magnetometer.

In our undertaking, a modified form of the coefficient for multiple determination $\tilde{R}^2$ was computed according to the formula for the single dipole model

$$\tilde{R}^2 = \frac{\sum_{i=1}^{m}\sum_{j=1}^{n}(\tilde{B}_{zij} - \bar{\tilde{B}}_{zij})^2 - \sum_{i=1}^{m}\sum_{j=1}^{n}(\tilde{B}_{zij} - \widehat{B}_{zij})^2}{\sum_{i=1}^{m}\sum_{j=1}^{n}(\tilde{B}_{zij} - \bar{\tilde{B}}_{zij})^2}$$

$$= 1 - \frac{\sum_{i=1}^{m}\sum_{j=1}^{n}(\tilde{B}_{zij} - \widehat{B}_{zij})^2}{\sum_{i=1}^{m}\sum_{j=1}^{n}(\tilde{B}_{zij} - \bar{\tilde{B}}_{zij})^2} \tag{45}$$

and

$$\tilde{R}^2 = \frac{\sum_{i=1}^{m}\sum_{j=1}^{n}(\tilde{B}_{zij} - \bar{\tilde{B}}_{zij})^2 - \sum_{i=1}^{m}\sum_{j=1}^{n}(\tilde{B}_{zij} - \widehat{B}_{zij} - \breve{B}_{zij})^2}{\sum_{i=1}^{m}\sum_{j=1}^{n}(\tilde{B}_{zij} - \bar{\tilde{B}}_{zij})^2}$$

$$= 1 - \frac{\sum_{i=1}^{m}\sum_{j=1}^{n}(\tilde{B}_{zij} - \widehat{B}_{zij} - \breve{B}_{zij})^2}{\sum_{i=1}^{m}\sum_{j=1}^{n}(\tilde{B}_{zij} - \bar{\tilde{B}}_{zij})^2} \tag{46}$$

for the two dipole model. As one can notice, the total magnetic field formula above does not have a zero-order term. This is because a bandpass, second-order digital Butterworth filter was employed to isolate the signal of interest and noise was thus assumed to have been eliminated. For the stomach, the passband used was

$$\frac{1}{60} \times 10^{-2} < \omega < \frac{7}{60} \times 10^{-2}. \tag{47}$$

where ω is the frequency of the signal. Applying the Butterworth filter motivated us to assume that contributions to **B** measurements due to the electrical activity of other organs, such as the brain and heart, had also been eliminated from our analysis because the signal due to these organs is characterized by a different range of frequencies.

The spatial arrangement of the co-planar magnetometer input channels corresponds to the locations in space where **B** values were recorded. These positions were modeled to lie in the plane $z = 0$ (m), directly above the abdominal region of the stomach. The volume under the upper section of the input grid determined by the SQUID input channels was assumed to contain the gastric current dipole while the one under the lower section was examined to identify a intestinal dipole. After applying the inverse problem algorithm, a statistical analysis was performed to determine the goodness of fit and thus test the appropriateness of the theoretical model developed. This was also done for the single dipole to determine which of the two models was simplest and most appropriate.

The experimental data sets selected for this statistical study consisted of magnetic field recordings taken at 200 Hz, spanning a total of two minutes of gastrointestinal electrical activity. As results suggest, the theoretical two-dipole model proposed does account for a significant proportion of the experimental data recorded. To quantify this statistically, a data analysis summary is provided in Table I, where one can notice that 50% of all $\tilde{R}^2$ values fall within (0.8720, 0.9731) for the first one-minute time interval of data sampling and within (0.6595, 0.9241) for the second. Comparatively, the interquartile ranges for the value of $\tilde{R}^2$ using the one-dipole model were found to be (0.6800, 0.7912) and (0.7418, 0.7869) for the two time intervals, respectively. Thus, as one can conclude, adding one dipole to the model produces the better approximation, as expected. Moreover, as the statistical figures presented above imply, the intestinal dipole is only responsible for a much smaller amount of the magnetic field values recorded as compared to the gastric dipole. This is also in agreement with the known characteristics of gastric and intestinal electrical activity. The results obtained are particularly encouraging in light of the

Table I. Data analysis summary of $\tilde{R}^2$ analysis for two randomly-chosen time segments of gastric biomagnetic field data. Results are shown for the single-dipole model (a) as well the two-dipole model (b)

Time segment	Minimum	First quartile	Mean	Median	Third quartile	Maximum
(a) Single-dipole model						
1	0.0025	0.6800	0.7635	0.7460	0.7911	0.9589
2	0.0032	0.7418	0.7652	0.7418	0.7869	0.8742
(b) Two-dipole model						
1	0.0005	0.8720	0.7189	0.9320	0.9731	0.9989
2	0.0094	0.6595	0.6923	0.8729	0.9241	0.9962

Table II. Sample deciles for $\tilde{R}^2$ computed for the reconstructed biomagnetic data using the single-dipole model (a) and the two-dipole model (b). Notice that the value of the 10th quantiles of the distribution are slightly higher than the means, which is due to the presence of outliers in the left tail for both time intervals of the sample

Decile	Time interval 1	Time interval 2
(a) Single-dipole model		
10	0.3635	0.7087
20	0.5014	0.7349
30	0.7183	0.7473
40	0.7473	0.7567
50	0.7634	0.7651
60	0.7749	0.7739
70	0.7856	0.7821
80	0.7984	0.7918
90	0.8084	0.8078
(b) Two-dipole model		
10	0.7289	0.4826
20	0.8424	0.6797
30	0.8885	0.8249
40	0.9117	0.8595
50	0.9279	0.8925
60	0.9554	0.9124
70	0.9692	0.9277
80	0.9766	0.9392
90	0.9866	0.9941

information in Table II, where one can see that the 10th and 20th deciles occur at sufficiently high values of $\tilde{R}^2$ to conclude that the theoretical model is quite accurate in explaining the biomagnetic field activity in the GI tract.

As far as the single-dipole model is concerned, Table II (b) suggests that the value of $\tilde{R}^2$ is low for a much larger number of time frames taken into consideration. For example, less than 10% of $\tilde{R}^2$ values are under 0.7 for the two-dipole model while over 25% of them are less than 0.7 for the single dipole case. Finally, the probability histograms for the empirical distributions of $\tilde{R}^2$ referring to the experimental data set including both time samples are depicted in Figure 1 (a) and (b). In these two cases also, one can see that the theoretical model developed is quite successful in describing the biomagnetic physiology of the stomach and small intestine. This figure is also suitable for performing a visual comparison of the effect of adding a second current dipole in the theoretical model. In addition to the $\tilde{R}^2$ analysis, the distribution of the sample error mean square for the two models was plotted and found to display the skewness characteristics found in lognormal, χ^2, or

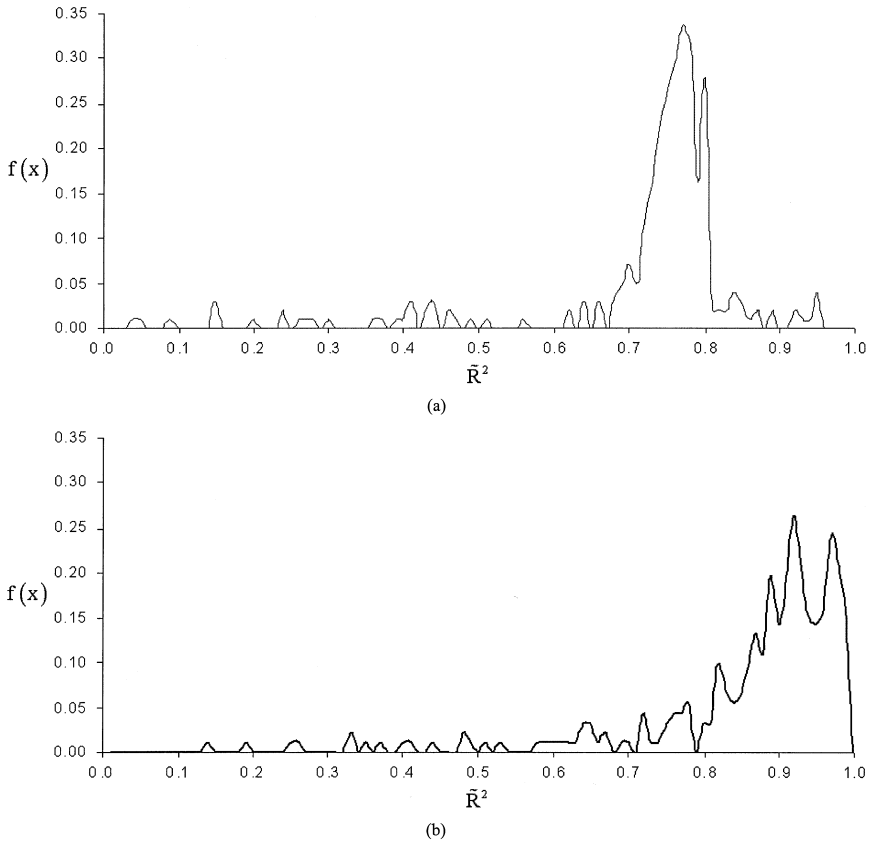

Figure 1. Empirical distribution of $\tilde{R}^2$ for time intervals 1 and 2 combined, accounting for two minutes of magnetic field recordings. Results for the single dipole model are shown in (a) and those for the two-dipole model in (b). The probability for a certain value of $\tilde{R}^2$ to occur is plotted on the abscissa and $\tilde{R}^2$ values are shown on the ordinate. As one can see by comparing (a) and (b) visually, the intestinal dipole is weaker and may account for roughly 15–25% of the observed magnetic field.

F-distributions, as shown in Figure 2. This was also the case in the one-dipole model, as expectable. For example, the standard error involved in the regression of the ith parameter was found from

$$\text{S.E.}\,(Q_i) = \frac{Q_i}{\sqrt{\hat{\sigma}^2 M_{ii}}} \tag{48}$$

where, according to standard regression analysis theory, M_{ii} is the element on the diagonal of the 4×4 matrix

$$\mathbf{M} = [(\mathbf{TAW})^T(\mathbf{TAW})]^{-1} \tag{49}$$

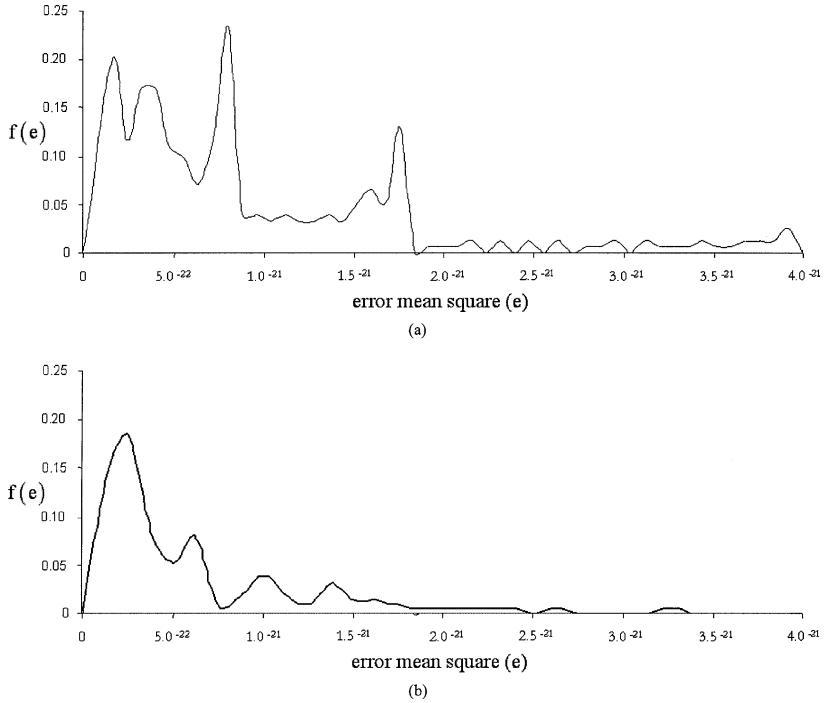

Figure 2. Empirical distribution function $f(e)$ for the error mean square of reconstructed biomagnetic field data for two minutes of recordings. The charts in (a) and (b) correspond to the single and two-dipole models, respectively.

corresponding to the ith parameter. Displayed in Table III is the significance of the estimated terms $\widehat{Q}_x$, $\widehat{Q}_y$, $\breve{Q}_x$ and $\breve{Q}_y$, which was found to be very large based on the ratio of the estimated parameters to their standard error.

5. Discussion

Modeling the GEA with accuracy and realism is an interesting theoretical and computational problem. Although a number of models have been proposed [7–18 20–22, 25] to simulate this phenomenon since the time when it was first detected by Alvarez [1], it can be difficult to ascertain which of them captures the characteristics of gastric activity most vividly. For example, coupled relaxation oscillator models [20–22] are also suitable for studying the time evolution of smooth muscle propagation, while dipole models are more appropriate for the investigation of electrical source uncoupling. In the past, modeling the GEA using electric current dipoles led to two important predictions, namely that the natural electrical control activity (ECA) frequency gradient may be detected noninvasively using magnetomers and also that ECA propagation in gastric musculature results in propagating patterns of

Table III. Significance of estimated parameters in the single-dipole (a) and two-dipole (b) gastric propagation model for a randomly selected time frame of magnetic field recordings for which $\tilde{R}^2 = 0.9766$ and the error mean square is equal to $\sigma^2 = 1.6349 \times 10^{-22}$

Parameter name $(Q_1, \ldots, Q_4)$	Parameter value	S.E. (Q_i)	Q_i/S.E. (Q_i)
(a)Single-dipole model			
$\widehat{Q}_x$	-9.7598×10^{-6}	2.2372×10^{-27}	4.3625×10^{-21}
$\breve{Q}_y$	-2.1849×10^{-6}	1.8252×10^{-27}	3.9879×10^{-21}
(b) Two-dipole model			
$\widehat{Q}_x$	-8.9824×10^{-6}	5.4067×10^{-25}	-1.6613×10^{-19}
$\widehat{Q}_y$	-6.9622×10^{-7}	9.2134×10^{-25}	-7.5566×10^{-17}
$\breve{Q}_x$	2.0998×10^{-6}	4.5212×10^{-25}	4.6445×10^{-17}
$\breve{Q}_y$	-3.5361×10^{-6}	8.2460×10^{-25}	-4.2882×10^{-18}

magnetic fields [3, 4]. Nevertheless, the present study is the first one to statistically compare GI models in terms of the number of dipoles used. Moreover, it is the first one to allow a direct assessment of which GI electric sources are most important statistically. Investigating the GEA from magnetic field recordings is encouraging due to the finding that, although magnetic field strengths decrease rapidly with distance from their sources, they do reveal the characteristics of these sources in a more accurate manner [3, 4].

In the case of magnetic fields originating in the brain and heart, the use of one-dipole models is sufficient due to the fact that detectors are located in the far field of compact sources of current. In GI investigations, however, where **B** fields are recorded in regions where more than one such source is present, it is difficult to determine the optimal model to be employed for best characterizing the electrical activity of the studied organs. Moreover, due to the complexity of the GI tract, it is necessary to find an accurate measure of a model's realism that would allow for its straightforward evaluation in terms of realism and usefulness. Due to the complex nature of the GI biomagnetic problem, it is essential to determine the extent to which a theoretical dipole model can be simplified without loss of realism and generality. Our study is thus meant to clarify these important issues and answer the relevant questions raised above. In a previous study [3, 4], gastric and intestinal magnetic fields were modeled using a spatio-temporal simulation in which 176 dipoles distributed along the GI tract were considered. Although this approach proved useful for demonstrating that diseased states of the stomach and small bowel could be detected from magnetic field measurements using SQUID magnetometers, a realistic experimental analysis was also necessary to determine the simplest and best model that could be used in the analysis of similar data acquired from humans. Moreover, in spite of our ability

to identify ECA propagation using this simulation, the complexity of the 176-dipole model made it difficult to isolate and study simulated magnetic field sources from inverse solutions. This particular aspect of the investigation is quite important due to the potential ability to determine regions of anomalous current propagation noninvasively.

The most important feature of our present model and statistical analysis is its attempt to overcome the difficulties presented above and offer a qualitative and quantitative estimate of the optimal theoretical and computational model to be used in clinical studies in which the GEA is investigated from magnetometer recordings. Our finding that the magnetic field signal attributed to one gastric current dipole accounts for more than half of the experimental **B** data recorded with a magnetometer is consistent with previous experimental and simulation results [3, 4], in that the magnetic field signal of the stomach is expected to be far stronger than the signal of the small bowel. Furthermore, our statistical results in support of choosing a two-dipole model for the entire tract constitutes a great simplification over the previous use of 176 dipoles and also enables one to contemplate investigations of the electromagnetic phenomena in these organs in a more straightforward fashion. The progress in studying the GEA from **B** field measurements reported in this article is relevant particularly because standard imaging techniques such as SPECT or PET are unable to convey information concerning the time evolution of electrical activity in the human abdomen.

6. Conclusions and Further Research

The task of identifying sources of electric current in the gastrointestinal tract can be important in the attempt to identify pathological conditions in humans at early stages. The theoretical and computational model that has been developed is promising from a computational perspective due to the straightforward approach taken in modeling the current sources and solving the inverse biomagnetic problem. The statistical analysis that has been performed shows that a two-dipole model is quite successful for modeling gastrointestinal electrical activity. An important addition to the model that indicates an interesting direction of investigation consists of allowing the depth of the current dipoles to vary, thus adding one extra degree of freedom to the mathematical model developed. Such a research effort may yield interesting results concerning the distribution of electric dipoles in those portions of the stomach that are more difficult to investigate noninvasively due to the inability of most instrumentation to distinguish the desired signal from biological noise. Since the differences in dipole locations and strengths between normal and pathological conditions are still unknown (October 2003), an important future application of our model can include a study of this important issue.

Acknowledgements

Financial support for this investigation was provided by the National Institute of Health, Grant R0 1 DK 58697-01A and by the Veteran Affairs Research Service, to which the authors are grateful.

References

1. Alvarez, W.C.: Electrogastrogram and What it Shows, *J. Am. Med. Assoc.* **78** (1922), 1116–1118.
2. Baillet, S., Mosher, J.C. and Leahy, R.M.: Electromagnetic Brain Mapping, *IEEE Signal Process. Mag.* **18**(6) (2001), 14–20.
3. Bradshaw, L.A., Allos, S.H., Wikswo, Jr., J.P. and Richards, W.O.: Correlation and Comparison of Magnetic and Electric Detection of Small Intestinal Electrical Activity, *Am. J. Physiol.* **35** (1997), G1159–G1167.
4. Bradshaw, L.A., Richards, W.O. and Wikswo, J. P.: Volume Conductor Effects on the Spatial Resolution of Magnetic Fields and Electric Potentials from Gastrointestinal Electrical Activity. *Med Biol. Eng. Comput.* **39** (2001), 35–43.
5. Daniel, E.E., Bardakjian, B.L., Huizinga, J.D. and Diamant, N.E.: Relaxation Oscillator and Core Conductor Models are Needed for Understanding of GI Electrical Activities, *Am. J. Physiol*. pt. 1, **266** (3) (1994), G339–G349.
6. Draper, N., Smith, H., *Applied Regression Analysis*, 2nd ed., Wiley & Sons, Inc., New York, 1981.
7. Familoni, B.O., Abel, T.A. and Bowes, K.L.: A Model of Gastric Electrical Activity in Health and Disease, *IEEE Trans. Biomed. Eng*. **42** (1995), 647–657.
8. Familoni, B.O., Kingma, Y.J., Bowes, K.L.: Noninvasive Assessment of Human Gastric Motor Function, *IEEE Trans. Biomed. Eng*. **34** (1987), 30–36.
9. Irimia, A.: Three-dimensional simulations of gastric biomagnetic dipoles using recursive localization algorithms. In: Proceedings of the IASTED International Conference on Applied Modeling and Simulation, Cambridge, Massachusetts, November 2–4, 2002, pp. 45–50.
10. Irimia, A.: Recursively-Applied Scanning Algorithms for Inverse Analyses of Gastrointestinal Biomagnetic Fields. In: Proceedings of the IASTED International Conference on Applied Modeling and Simulation, Cambridge, Massachusetts, November 2–4, 2002, pp. 51–55.
11. Irimia, A.: Theoretical models and biomathematical algorithms for identifying multiple gastrointestinal dipoles. In: Proceedings of the IASTED International Conference on Applied Modeling and Simulation, Cambridge, Massachusetts, November 2–4, 2002, pp. 56–61.
12. Kothapalli, B.: Electrogastrogram Simulation Using a Three-Dimensional Model, *J. Med. Biol. Eng. Comput*. **31** (1993), 482–486.
13. Larson, R.E., Hostetler, R.P., Edwards, B.H.: *Calculus with Analytic Geometry*, Alternate 5th ed., D. C. Heath & Co., Lexington, Massachusetts, 1994, pp. 348–349.
14. Mintchev, M.P., Bowes, K.L.: Conoidal Dipole Model of Electrical Field Produced by the Human Stomach, *Med. Biol. Eng. Comput*. **33**(2) (1995), 179–184.
15. Mintchev, M.P., Otto, S.J., Bowes, K.L.: Elecrogastrography can Recognize Gastric Electrical Uncoupling in Dogs. *Gastroenterology* **112**(6) (1997), 2006–2011.
16. Mirizzi, N., Stella, R. and Scafoglieri, U.: A Model of Extracellular Waveshapes of Gastric Electrical Activity, *Med. Biol. Eng. Comput*. **23** (1985), 33–37.
17. Mirizzi, N., Stella, R. and Scafoglieri, U.: Model to Simulate the Gastric Electrical Control and Response Activity on the Abdominal Wall and Abdominal Surface, *Med. Biol. Eng. Comput.* **24** (1986), 157–163.

18. Publicover, N.G., Sanders, K.M.: Are Relaxation Oscillators an Appropriate Model of the Gastrointestinal Electrical Activity? *Am. J. Physiol.* pt. 1, **256**(2) (1989), G265–G274.
19. Richards, W.O., Garrard, C.L., Allos, S.H., Bradshaw, L.A., Staton, D.J. and Wikswo Jr., J.P.: Noninvasive Diagnosis of Mesenteric Ischemia Using a SQUID Magnetometer, *Ann. Surg.* **221**(6) (1995), 696–705.
20. Sarna, S.K.: Daniel, E.E. and Kingma, Y.J.: Simulation of the Electrical Activity of the Stomach by an Array of Relaxation Oscillators, *Dig. Dis.* **17** (1972), 299–310.
21. Sarna, S.K.: Models of smooth muscle electrical activity, in E.E. Daniel and D.M. Paton (eds.) *Methods in Pharmacology, Smooth Muscle*, Plenum, New York, 1975, pp. 519–540.
22. Sarna, S.K.: *In vivo* myoelectric activity: Methods, analysis and interpretation, in S.G. Schultz and J.D. Wood (eds.) *Handbook of Physiology: Gastrointestinal System: Motility and Circulation*, American Physiological Society, Bethesda, MD, 1989, pp. 817–863.
23. Sarvas, J.: Basic Mathematical and Electromagnetic Concepts of the Biomagnetic Inverse Problem, *Phys. Med. Biol.* **32**(1) (1987), 11–22.
24. Young, P.: Recursive Estimation and Time-Series Analysis—An Introduction, Springer-Verlag, New York, 1984.
25. Wang, Z.S., Cheung, J.Y., Gao, S.K. and Chen, J.D.Z.: Spatio-Temporal Nonlinear Modeling of Gastric Myoelectrical Activity, *Methods Inf. Med.* **39**(2) (2000), 186–190.